

# Maximum cooling and maximum efficiency of thermoacoustic refrigerators

L. K. Tartibu<sup>1</sup>

Received: 3 December 2014 / Accepted: 27 May 2015 / Published online: 3 June 2015  
© Springer-Verlag Berlin Heidelberg 2015

**Abstract** This work provides valid experimental evidence on the difference between design for maximum cooling and maximum efficiency for thermoacoustic refrigerators. In addition, the influence of the geometry of the honeycomb ceramic stack on the performance of thermoacoustic refrigerators is presented as it affects the cooling power. Sixteen cordierite honeycomb ceramic stacks with square cross sections having four different lengths of 26, 48, 70 and 100 mm are considered. Measurements are taken at six different locations of the stack hot ends from the pressure antinode, namely 100, 200, 300, 400, 500 and 600 mm respectively. Measurement of temperature difference across the stack ends at steady state for different stack geometries are used to compute the cooling load and the coefficient of performance. The results obtained with atmospheric air showed that there is a distinct optimum depending on the design goal.

## Abbreviations

a	Speed of sound (m/s)
BR	Blockage ratio
COP	Coefficient of performance of refrigerator
COPC	Carnot coefficient of performance
COPR	Relative coefficient of performance
DR	Drive ratio
f	Frequency (Hz)
K	Thermal conductivity (W/m K)
l	Plate half thickness (mm)

$L_S$	Stack length (mm)
$L_{Sn}$	Normalised stack length
$p_m$	Mean pressure (Pa)
$T_m$	Mean temperature
$T_{mn}$	Normalized temperature difference
$X_S$	Stack centre position (mm)
$X_{Sn}$	Normalised stack position
$y_o$	Plate half-gap (mm)
$\delta_k$	Gas thermal penetration depth (mm)
$\delta_{kn}$	Normalised thermal penetration depth
$\gamma$	Isentropic coefficient
$\varepsilon_s$	Stack heat capacity correction factor
$\omega$	Angular frequency (rad/s)
$\rho_m$	Density (kg/m <sup>3</sup> )
$\sigma$	Prandtl number
$\theta$	Normalised temperature difference
$\Delta T_m$	Temperature span (K)
$\Phi_C$	Normalized cooling load
$\Phi_H$	Normalized heat flow
$\Phi_W$	Normalized acoustic power
$\mu$	Dynamic viscosity (kg/m s)
$\lambda$	Wavelength (mm)

## 1 Introduction

Thermoacoustics is a field of study that combines both acoustic waves and thermodynamics. The interaction of the temperature oscillation accompanied by the pressure oscillation in a sound wave with solid boundaries initiates an energy conversion processes. In ordinary experience, this interaction between heat and sound cannot be observed. But it can be amplified under suitable conditions to give rise to significant thermodynamic effects such as convective heat fluxes, steep thermal gradients and strong sound

✉ L. K. Tartibu  
lagougetartibu@yahoo.fr

<sup>1</sup> Department of Mechanical Engineering Technology,  
University of Johannesburg, Doornfontein Campus,  
Johannesburg 2006, South Africa

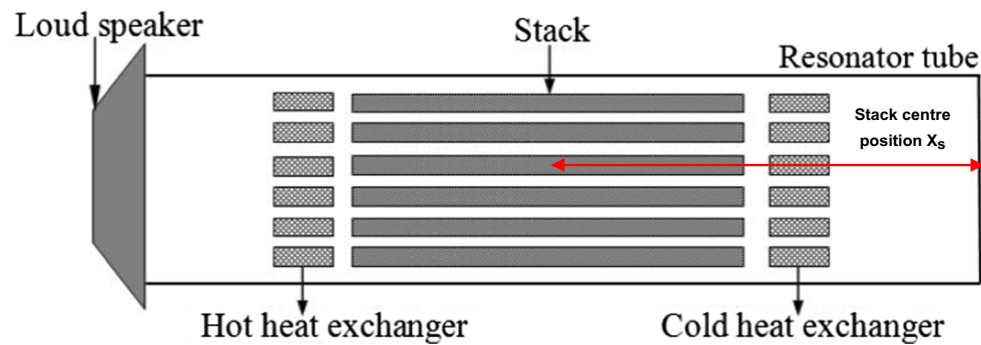
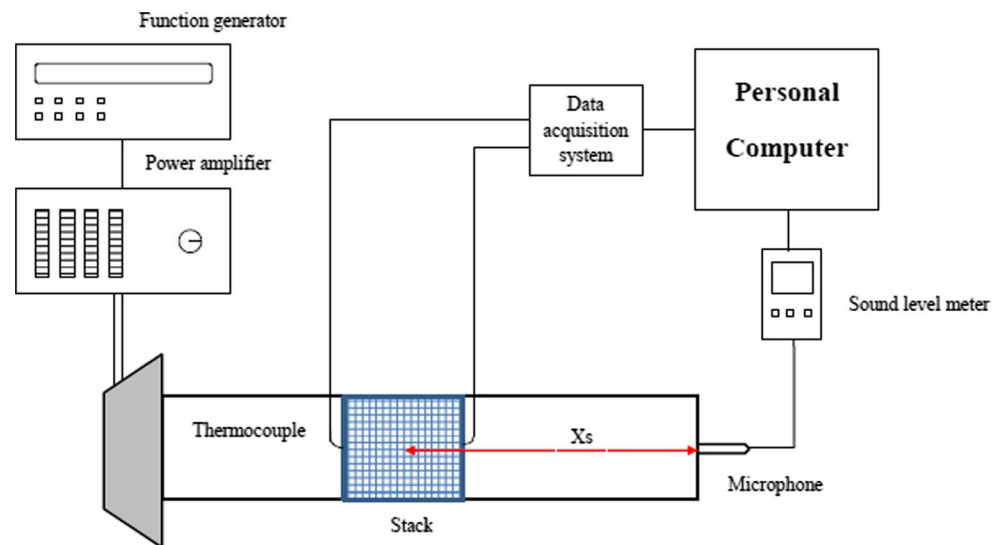


**Fig. 1** Schematic diagram of a typical thermoacoustic refrigerator

**Fig. 2** A schematic diagram of experimental apparatus



fields. Thermoacoustic refrigerators (TARs) use acoustic power to cause heat flow from a low temperature source to high temperature sink [1].

Thermoacoustic refrigerators (Fig. 1) consist mainly of a loudspeaker (a vibrating diaphragm or thermoacoustic prime mover) attached to a resonator filled with gas, a stack usually made of thin parallel plates, and two heat exchangers placed at either side of the stack. The stack forms the heart of the refrigerator where the heat-pumping process takes place, and it is thus a critical element for determining the performance of the refrigerator [2]. Using a sound source such as a loudspeaker, an acoustic wave is generated to make the gas resonant. As the gas oscillates back and forth within the chamber, the standing sound wave creates a temperature difference along the length of the stack (with the cold side located on the left hand side and the hot side on the right hand side in Fig. 1). This temperature change is a result of compression and expansion of gas by sound pressure and thermal interaction between the oscillating gas and the surface of the plate (Fig. 2).

To understand the heat transfer, the oscillatory gas thermodynamics and achieve highest performance, fundamental research is required that addresses several important problems in thermoacoustic systems. These problems include temperature fields in system elements, evaluation of coefficient of performance and cooling load in order to illustrate the viscous and thermal losses within the porous media stacks. Most importantly, the design for maximum cooling and maximum coefficient of performance do not coincide [3, 4]. While the former is far away from the closed end, the latter is close to it. For electronic cooling (small-scale devices), the main objective is to achieve highest cooling loads, while maximising the coefficient of performance, is the goal for large-scale devices.

## 2 Motivations

To evaluate the thermal performance, the temperature differences across the stack end temperature have been measured. Several authors [5–10] have studied the temperature

**Table 1** Normalised cooling load and acoustic power

Operation parameters	
Normalised cooling power	$\Phi_H = \frac{\dot{Q}_c}{p_m a A}$
Normalised acoustic power	$\Phi_W = \frac{\dot{W}}{p_m a A}$

difference at the stack extremities either mathematically, numerically or experimentally in order to improve the performance of thermoacoustic refrigerators through the use of optimisation. But there are no explicit experimental studies in the literature about the design choice between maximum cooling and maximum coefficient of performance as highlighted in references [3, 4] using mathematical approaches. Therefore, the present work aims to provide experimental evidence on the difference between design for maximum cooling and maximum coefficient of performance of thermoacoustic refrigerator. The remainder of this paper is organized in the following fashion: in Sects. 3 and 4, the design parameters of thermoacoustic core and objectives are presented. Experimental set-up and apparatus are described in Sect. 5. Sections 6 and 7 report the contributions of this work.

### 3 Design parameters of the thermoacoustic core

The basic design requirements for thermoacoustic refrigerator are twofold [3]:

(1) to supply the desired cooling load ( $\dot{Q}_c$ ); and (2) to achieve the prescribed cooling temperature ( $T_c$ ) or a given temperature difference ( $\Delta T$ ) over the stack at the same time.

The resultant normalised operation parameters are presented in Table 1. The number of parameters can be reduced by making a choice of some normalised parameters.

The coefficient of performance of a thermoacoustic core COP is dependent on 19 independent design parameters [11]. Herman and Travnicek [3] have collapsed the number of parameters to the following six normalised parameter spaces, as shown in Table 2.

### 4 Design objectives

The performance of the thermoacoustic stack depends on three main stack design parameters: (1) the centre position, (2) the length, and (3) the cross-section area of the stack. The normalised cooling power ( $\Phi_H$ ) and acoustic power ( $\Phi_W$ ) neglecting axial conduction in the working fluid as well as in the stack plates are given as follows [12]:

$$\Phi_H = - \left[ \frac{\delta_{kn} DR^2 \sin(2X_{Sn})}{8\gamma(1+\sigma) \left(1 - \sqrt{\sigma}\delta_{kn} + \frac{1}{2}\sigma\delta_{kn}^2\right)} \right] \times \left[ \frac{\Delta T_{mn} \tan(X_{Sn})}{(\gamma-1)BR L_{Sn}} \times \frac{(1+\sqrt{\sigma}+\sigma)}{1+\sqrt{\sigma}} - (1+\sqrt{\sigma}-\sqrt{\sigma}\delta_{kn}) \right] \quad (1)$$

$$\Phi_W = \left[ \frac{\delta_{kn} DR^2 L_{Sn} (\gamma-1) BR \cos^2(X_{Sn})}{4\gamma} \right] \times \left[ \frac{\Delta T_{mn} \tan(X_{Sn})}{BR L_{Sn} (\gamma-1) (1+\sqrt{\sigma}) \left(1 - \sqrt{\sigma}\delta_{kn} + \frac{1}{2}\sigma\delta_{kn}^2\right)} - 1 \right] - \left[ \frac{\delta_{kn} L_{Sn} DR^2}{4\gamma} \times \frac{\sqrt{\sigma} \sin^2(X_{Sn})}{BR \left(1 - \sqrt{\sigma}\delta_{kn} + \frac{1}{2}\sigma\delta_{kn}^2\right)} \right] \quad (2)$$

The normalised cooling load ( $\Phi_C$ ), the coefficient of performance of the thermoacoustic core COP and the

**Table 2** TAR parameters

Operation parameters	
Drive ratio (DR)	$DR = \frac{p_0}{p_m}$ where $p_0$ and $p_m$ are respectively the dynamic and mean pressure
Normalised temperature difference	$\theta = \Delta T_{mn} = \frac{\Delta T_m}{T_m}$ where $\Delta T_m$ and $T_m$ are respectively the desired temperature span and the mean temperature span
Gas parameters	
Normalised thermal penetration depth	$\delta_{kn} = \frac{\delta_k}{y_0}$ where $2y_0$ is the plate spacing
Stack geometry parameters	
Normalised stack length	$L_{Sn} = \frac{2\pi f}{a} L_S$ where $L_S$ the stack length
Normalised stack position	$X_{Sn} = \frac{2\pi f}{a} X_S$ where $f$ , $a$ and $X_S$ are respectively the resonant frequency, the speed of sound and the stack centre position
Blockage ratio or porosity	$BR = \frac{y_0}{(y_0+l)}$ where $2l$ is the plate thickness

coefficient of performance relative to Carnot can be defined respectively as follows [11]:

$$\Phi_C = \Phi_H - \Phi_W \quad (3)$$

$$\text{COP} = \frac{\Phi_H - \Phi_W}{\Phi_W} \quad (4)$$

$$\text{COPR} = \frac{\text{COP}}{\text{COP}_C} = \frac{(|\Phi_H| - |\Phi_W|)/|\Phi_W|}{(2 - \theta)/(2\theta)} \quad (5)$$

## 5 Experimental investigation

### 5.1 Experimental set-up

The main objectives of this experimental scheme are to obtain the following characteristics of the stack:

- measurements of temperature difference ( $\Delta T$ ) obtained across the stack ends at steady state for different stack geometries (lengths of the stacks varying from 26 to 100 mm) and stack spacing (homogenous stacks ranging from 64 to 300 Cells Per Square Inch, or CPSI).
- measurements of the temperature difference ( $\Delta T$ ) obtained across the stack ends at steady state for different positions of the stack (the hot end of the stack varies from 100 to 600 mm from the closed end).
- Compute the cooling load  $\Phi_c$  and the coefficient of performance relative to Carnot COPR in each cases.

The TAR experimentation was carried out using a quarter-wavelength resonator design. A speaker-driven system was used to ensure equal acoustic environments for each test instead of a heat driven one. An experimental set-up (thermoacoustic refrigerator) for measuring the performance of the device function of the geometry of the stack has been designed and assembled. The set-up has the following components:

- a resonator tube;
- a loudspeaker; and
- a stack.

As this set-up does not have hot heat exchanger and cold heat exchanger at the ends of the stack, it is similar to a thermoacoustic couple (TAC). For this study, the stack is not cooled actively. The main function of this experiment is to compare optimal design for maximum cooling to the design for maximum efficiency, rather than achieving highest temperature drop or cooling power.

The resonator is an acrylic tube (thermal conductivity 0.20 W/m K at 23 °C) of a length of 780 mm and an inner diameter of 44 mm. The resonator is filled with air at atmospheric pressure. The position of the stack can be

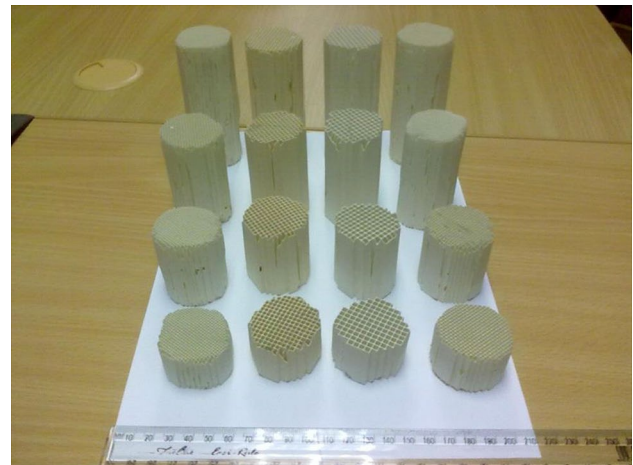


**Fig. 3** Stack samples used in the experiments

adjusted at any location on the resonator. One end of the tube is closed with an end cap. At the other end, a commercially available loudspeaker (4  $\Omega$ ) constitutes the acoustic power source (driver). The loudspeaker has a frequency range of 45–26,000 Hz and 180 W maximum acoustic power output. This driver is located in PVC housing (130  $\times$  130  $\times$  72 mm) to which the resonator is connected. A function generator (model Agilent 33220A) and an 80 W amplifier have been used to drive the system at the operating frequency and with the selected power. The accuracy of the amplitude and the frequency of the output signal are 0.1 mV and 1  $\mu$ Hz, respectively.

The stacks studied in the measurement set-up are pre-fabricated stacks made of 64, 100, 230 and 300 CPSI respectively, manufactured by Applied Ceramics Inc. [13]. The cordierite honeycomb ceramic is selected because of its low thermal conductivity, high surface area for conversion efficiency, high thermal capability (up to 1400 °C), ability to sustain large temperature gradients and highest sound pressure level output. Additionally, such stacks are relatively cheaper and easier to make, especially when the channel size goes down into tens of microns range. Sixteen cordierite honeycomb ceramic stacks with square cross sections (as shown in Fig. 3) having four different lengths—26, 48, 70 and 100 mm—are considered. Cordierite honeycomb ceramic stack properties and specifications are provided in Table 3. Measurements are taken at six different locations of the stack hot ends from the pressure antinode, namely 100, 200, 300, 400, 500 and 600 mm respectively

### 5.2 Experimental apparatus

A variety of equipment is utilised to perform the measurements. Thermocouples are used to measure thermal

**Table 3** Properties and dimensions of stack materials [13]

Material: cordierite ceramic honeycomb				
Density (Kg/m <sup>3</sup> )	2500			
Thermal conductivity (W/m K)	0.42			
Specific heat (J/Kg K)	1047			
Melting point (°C)	1450			
Coefficient of thermal expansion °C × 10 <sup>-6</sup>	0.7			
Refrigerator				
Stack lengths (mm)	100			
	70			
	48			
	26			
Stack position (from closed end) (mm)	100			
	200			
	300			
	400			
	500			
	600			
Size (pore sizes)				
	Size 4: 64 CPSI	Size 3: 100 CPSI	Size 2: 230 CPSI	Size 1: 300 CPSI
Plate thickness (mm)	0.690	0.550	0.160	0.140
Plate spacing (mm)	3.175	2.540	1.675	1.467
Porosity (BR)	≈0.8	≈0.8	≈0.9	≈0.9

response, and pressure measurements are made with a sound level meter, while a data acquisition system records the measurements (as shown in Fig. 2).

A common method to record temperature is through the use of thermocouples. K-Type thermocouples wires have been selected for this work. They are made of chromel and alumel from National Instruments [14]. Based on National Instruments, these exposed junction type thermocouples which feature fiberglass insulation (melting point 482 °C) allow for a temperature range of 0–482 °C. The accuracy of the thermocouple is ±2.2 °C [14].

The acoustic pressure measurements are made by a sound level meter [15] which, when placed near the driver end, measures the dynamic pressure ( $P_0$ ). The drive ratio (DR) is evaluated using this dynamic pressure measurement. The accuracy of the sound level meter, as indicated by Lutron Electronic [15] is ±1.5 dB. To convert the sound level meter data from decibel (dB) to Pascal (Pa), the following expression is used:

$$L_p = 10 \log_{10} \left( \frac{P^2}{P_{ref}^2} \right) = 20 \log_{10} \left( \frac{P}{P_{ref}} \right) \text{ dB} \quad (6)$$

where  $L_p$  = sound pressure level in dB,  $P$  = root mean square sound pressure =  $\frac{P_0}{\sqrt{2}}$ ,  $P_{ref}$  =  $20 \times 10^{-6}$  Pa or 20  $\mu$ Pa = reference pressure.

The analog signals generated by sensors are obtained using data acquisition (DAQ) hardware (as shown in Fig. 2). Once these signals are interpreted by the DAQ, a digital signal is sent to a computer for processing, recording and analysing. Although there are numerous possible solutions for acquiring and processing analog data, LabVIEW 11 [16] has been selected as the environment for data visualisation and processing, together with a National Instruments (NI) DAQ hardware (NI USB-9211A).

A portable USB based DAQ is chosen for thermocouple measurement (National instruments hardware NI USB-9211). The sound level meter is a portable five digits, compact sized, digital display sound level meter designed for long term measurements, with an operating environment of 0–50 °C.

## 6 Results

### 6.1 Temperature behaviour as a function of driving frequency

In this set of experiments, the effect of the driving frequency on the temperature difference across the stack was investigated. During these experiments, the hot end of a 100 mm stack (size 2) remained 100 mm from the closed

end and the function generator voltage was kept at 150 m  $V_{\text{RMS}}$ . The data for this test was collected beginning at 50 Hz and ranging up to 350 Hz in increments of 5 Hz. The response time of the temperature was much slower than the pressure amplitude; hence, each frequency was maintained for approximately 250–350 s. Figure 4 illustrates the hot side temperature, the cold side temperature and the temperature difference across the stack end as obtained and recorded in this study.

A second test was run with a frequency increment of 1 Hz, starting at 130 Hz and ranging beyond the first peak (140 Hz) in order to illustrate a more exact picture of the temperature behaviour in the range of frequencies present in the first peak. Figure 5 shows the temperature difference for the entire range of frequencies. The optimal driving frequency identified results in the highest temperature difference across the stack, as suggested by previous studies [8]. The total length of this TAR set-up was 780 mm, which corresponds to an optimal operating frequency of  $\approx 110$  Hz. This is not in agreement with the results reported in Fig. 5 evaluating the standing wave resonator frequency at 135 Hz. Similar findings are reported by Yong Tae Kim and Min Gon Kim [17] who suggest that the frequency of the peak temperature difference won't be in satisfactory agreement with the system resonance frequency if the stack position is not optimum. Therefore, all remaining results were taken under the same operating conditions, with the driving frequency fixed at 135 Hz.

## 6.2 Cooling load and Carnot coefficient of performance

The coefficient of performance (COP) of a thermoacoustic refrigerator indicates how effective the device is in converting and producing cooling load by absorbing sound energy. Therefore the coefficient of performance is given by Eqs. 4 and 5. The cooling power, the acoustic power and the cooling load are calculated respectively using Eqs. 1–3. Table 4 presents the parameters as estimated for the cordierite honeycomb ceramic stack used in this experiment. The normalised values are obtained from Tables 2 and 3.

For all the stack lengths considered, the values of COPR decrease as the distance from the pressure antinode (closed end) increases (Figs. 6, 7, 8, 9). In particular, the shortest stack length shows the highest COPR for Figs. 6, 7 and 9 corresponding respectively to sizes 1, 2 and 4. Interestingly, this behaviour has been observed by Herman and Travnicek [3] and Tartibu et al. [4] using mathematical modelling. From Eq. 2, the acoustic power is proportional to the length of the stack and the viscous loss is increased as the velocity amplitude increases. Therefore, a shorter stack length absorbs less acoustic power and exhibits higher COPR. These findings are useful for the design of large-scale devices.

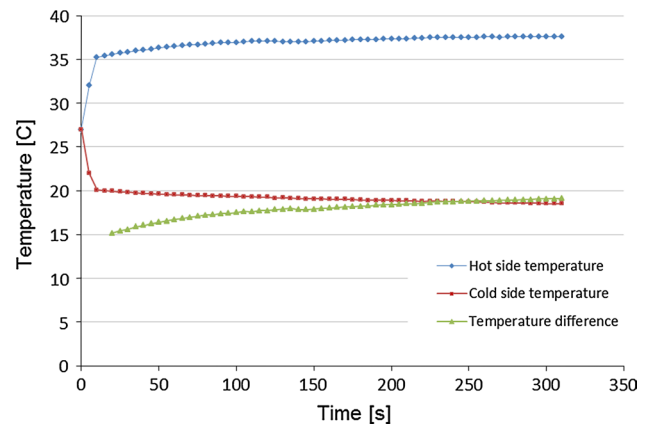


**Fig. 4** Hot side and cold side temperature across the ceramic stack/TAR

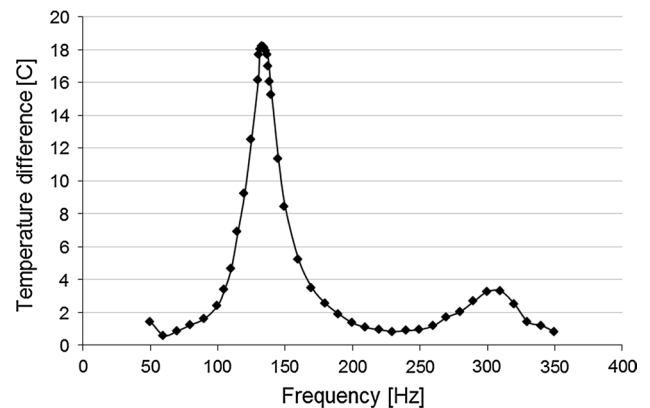


**Fig. 5** Temperature difference function of the frequency

The COPR presented in this study is roughly 70 % of Carnot COP. While considering the losses (viscous and thermal) along the stack, the heat exchangers, the resonator, the heat leaks through the stack and the resonator and the efficiency of a loudspeaker, the COPR of a complete thermoacoustic refrigerator will be lower than the COPR of a stack as presented in this study.

## 6.3 Cooling load

Figures 10, 11, 12 and 13 represent the cooling load function of the normalised stack centre position. There is maximum cooling load when the stack is moved away from the pressure antinode. The results suggest the cooling load increases with the stack length. Contrary to the maximum COPR presented in Figs. 6, 7, 8 and 9, increasing the stack length leads to an increase in cooling load for TAR. This concurs with previous studies by Herman and Travnicek [3] and Tartibu et al. [4] suggesting that there is a distinct optimum for maximum cooling and maximum coefficient

**Table 4** Estimated parameters of TAR

L <sub>sn</sub>		X <sub>sn</sub>		δkn	F (Hz)	T <sub>m</sub> (K)	DR
0.065	0.280	0.528	0.777	1.024	1.272	1.520	0.135
0.119	0.307	0.555	0.803	1.051	1.299	1.547	0.168
0.173	0.334	0.582	0.830	1.078	1.326	1.574	0.255
0.248	0.372	0.620	0.868	1.116	1.364	1.612	0.291

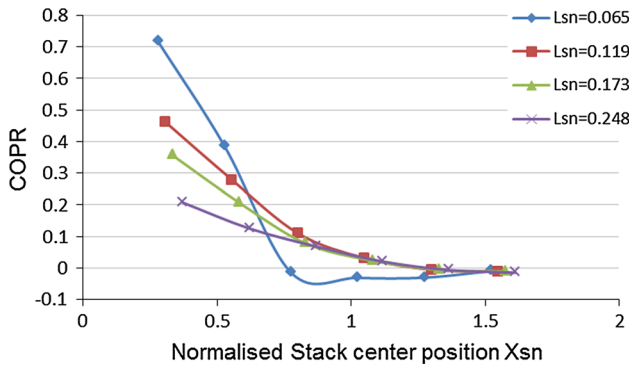


**Fig. 6** COPR for size 1 honeycomb ceramic stacks

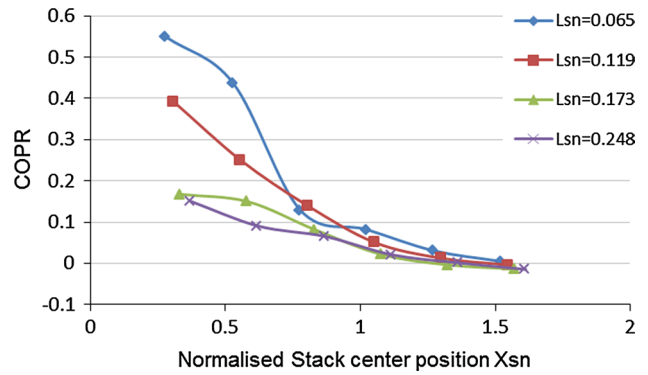


**Fig. 9** COPR for size 4 honeycomb ceramic stacks

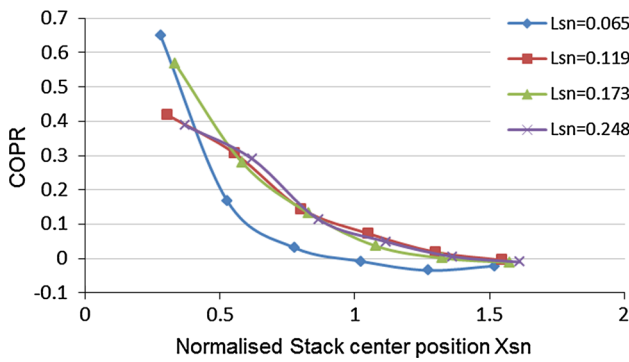


**Fig. 7** COPR for size 2 honeycomb ceramic stacks

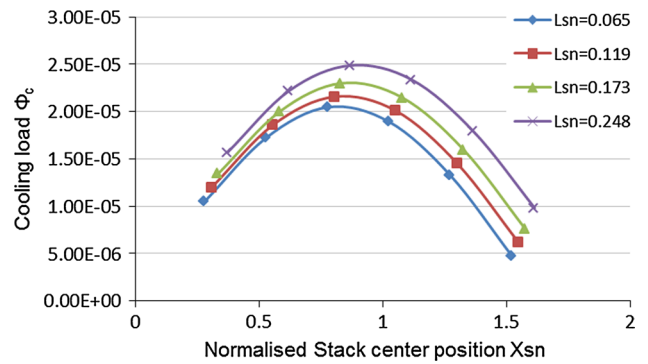


**Fig. 10** Cooling load for size 1 honeycomb ceramic stacks

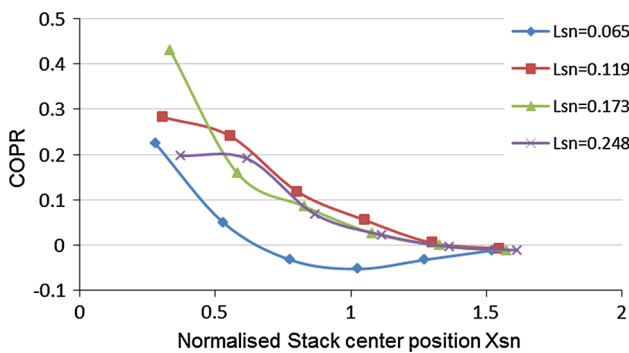


**Fig. 8** COPR for size 3 honeycomb ceramic stacks

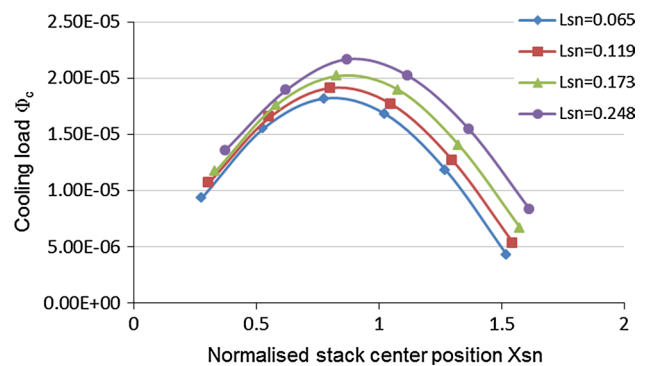


**Fig. 11** Cooling load for size 2 honeycomb ceramic stacks

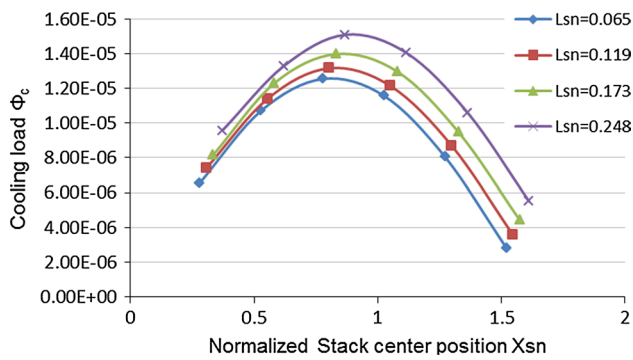


**Fig. 12** Cooling load for size 3 honeycomb ceramic stacks

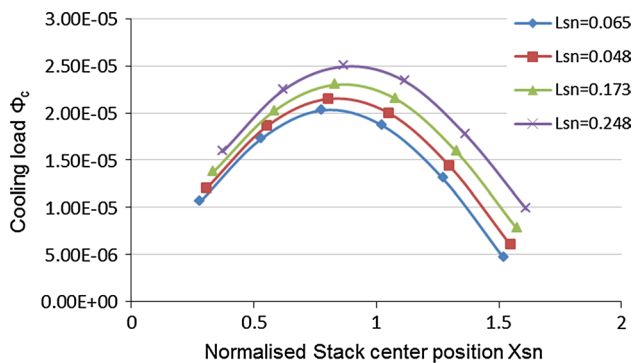


**Fig. 13** Cooling load for size 4 honeycomb ceramic stacks

of performance. One will suspect that the normalized stack length  $L_{Sn}$  and the normalized stack position  $X_{Sn}$  are somehow related. Indeed, that is the case. These findings are useful for the design of small-scale devices.

## 7 Conclusion

In order to investigate the influence of stack geometry and position on the performance of the device, an acoustically driven thermoacoustic refrigerator was built. This system utilises a loudspeaker to create strong sound waves in a quarter wavelength resonator. Sixteen different cordierite honeycomb ceramic stacks of four different pore sizes were investigated. These stacks were moved successively at six different locations inside the resonator. The temperature differences across the stack in each configuration were used to measure the performance of the refrigerator. The data obtained were used to calculate the coefficient of performance and the cooling load. While locating the stack closer to the pressure antinode for maximum coefficient of performance of the device is confirmed through this study,

the design for maximum cooling implies moving the stack away from the pressure antinode. This present study reveals and quantifies that the results obtained with these two design goals are different. There is a specific stack geometry and position for maximum performance of the devices depending on the device size.

**Acknowledgments** This research was supported by the Research office of Mangosuthu University of Technology, Durban, South Africa.

## References

1. Swift GW (2002) Thermoacoustics: a unifying perspective for some engines and refrigerators. Acoustical Society of America, Melville
2. Swift GW (1988) Thermoacoustic engines. *J Acoust Soc Am* 4:1146–1180
3. Herman C, Travnicek Z (2006) Cool sound: the future of refrigeration? Thermodynamic and heat transfer issues in thermoacoustic refrigeration. *Heat Mass Transf* 42(6):492–500
4. Tartibu LK, Sun B, Kaunda MAE (2014) Lexicographic multi-objective optimisation of thermoacoustic refrigerator's stack. *J Heat Mass Transf* 51:649–660. doi:10.1007/s00231-014-1440-z
5. Atchley AA, Hoffer TJ, Muzzerall ML, Kite MD (1999) Acoustically generated temperature gradients in short plates. *J Acoust Soc Am* 88:251–263
6. Worlikar AS, Knio OM, Klein R (1998) Numerical simulation of a thermoacoustic refrigerator: stratified flow around the stack. *J Comput Phys* 144:299–324
7. Marx D, Blanc-Benon P (2005) Numerical calculations of the temperature difference between the extremities of a thermoacoustic stack plate. *Cryogenics* 45:163–172
8. Zink F (2009) Identification and attenuation of losses in thermoacoustics: issues arising in the miniaturization of thermoacoustic devices. Ph.D. thesis, University of Pittsburgh, United States
9. Tu Q, Chen ZJ, Liu JX (2005) Numerical simulation of loudspeaker-driven thermoacoustic refrigerator. Proceedings of the twentieth international cryogenic engineering conference (ICEC 20). Beijing, China
10. Akhavanbazaz M, Siddiqui MK, Bhat RB (2007) The impact of gas blockage on the performance of a thermoacoustic refrigerator. *Exp Therm Fluid Sci* 32(1):231–239
11. Wetzel M, Herman C (1997) Design optimisation of thermoacoustic refrigerators. *Int J Refrig* 20(1):3–21
12. Tijani MEH, Zeegers JCH, De Waele ATAM (2002) Design of thermoacoustic refrigerators. *Cryogenics* 42(1):49–57
13. Applied Ceramics Inc. (2011) Versagrid™ product offering. [http://appliedceramics.com/products\\_versagrid.htm](http://appliedceramics.com/products_versagrid.htm). Accessed 10 Sept 2013
14. National Instruments (2013) Thermocouple and RTD sensors. <http://www.ni.com/pdf/products/us/3daqsc350-351.pdf>. Accessed 10 Sept 2013
15. Lutron Electronic (2013) Sound level meter model SL-4013. [http://www.instrumentsgroup.co.za/index\\_files/Lutron/database/pdf/SL-4013.pdf](http://www.instrumentsgroup.co.za/index_files/Lutron/database/pdf/SL-4013.pdf). Accessed 10 Sept 2013
16. National Instruments (2011) <http://www.ni.com/labview/>
17. Yong Tae Kim & Min Gon Kim (2000) Optimum positions of a stack in a thermoacoustic heat pump. *J Korean Phys Soc* 36(5):279–286